Letter

Breaking of reciprocity and the Pancharatnam-Berry phase for light scattered by a disordered cold-atom cloud

P. H. N. Magnani,[1] P. G. S. Dias,[1] M. Frometa,[2] M. A. Martins,[1] N. Piovella,[3,4] R. Kaiser,[5] Ph. W. Courteille,[2] M. Hugbart,[5] R. Bachelard,[1,5] and R. C. Teixeira[1,*]

[1]*Departamento de Física, Universidade Federal de São Carlos, Rodovia Washington Luís, km 235 - SP-310, 13565-905 São Carlos, São Paulo, Brazil*

[2]*Instituto de Física de São Carlos, Universidade de São Paulo - 13566-590 São Carlos, São Paulo, Brazil*

[3]*Dipartimento di Fisica "Aldo Pontremoli," Università degli Studi di Milano, Via Celoria 16, I-20133 Milano, Italy*

[4]*INFN Sezione di Milano, Via Celoria 16, I-20133 Milano, Italy*

[5]*Université Côte d'Azur, CNRS, INPHYNI, 06200 Nice, France*

(Received 11 January 2024; revised 25 July 2024; accepted 26 September 2024; published 23 October 2024)

Collective effects on the light scattered by disordered media such as Anderson localization and coherent backscattering critically depend on the reciprocity between interfering optical paths. In this Letter, we explore the breaking of reciprocity for the light scattered by a disordered cold-atom setup, taking advantage of the noncommutation of optical elements that manipulate the polarization of the interfering paths. This breaking of symmetry manifests itself in the reduction of the fringes' contrast as the light scattered by the cloud interferes with that from its mirror image. We provide a geometrical interpretation in terms of the Pancharatnam-Berry phase, which we directly access from the fringe displacement. Our work paves the way toward the manipulation of path reciprocity and interference of light using atomic media, where it could be combined with collective and saturation effects.

DOI: 10.1103/PhysRevA.110.L041302

Introduction. Symmetries are fundamental properties of a system which determine the conserved quantities of its dynamics [1,2], thus setting constraints on its evolution. In particular, the charge, parity, and time-reversal (*CPT*) symmetry is universal as it applies to all known forces. Yet an important aspect of this symmetry is that it holds for a system as a whole, and considering the full symmetry, rather than a single one of the three. A simple illustration can be found in classical optics: While the *CPT* symmetry holds for the scattering of light by particles if one monitors all degrees of freedom, it breaks down as one focuses, for example, on the coherently scattered light. Indeed, the scattering of electromagnetic energy in other modes is typically encapsulated in the imaginary part of the medium refractive index, thus inducing a dissipative nature to the system. The necessity to differentiate absorption, which as a matter of fact defines an arrow for time and prevents the time-reversal symmetry, from other energy-preserving mechanisms which may break that symmetry, has led to the notion of reciprocity [3,4].

Reciprocity, in optics and beyond, describes the similarity of the transformations undergone by two waves traveling along the same path, yet in opposite directions. The fields emerging from these two "reciprocal paths" can be made to interfere, and in disordered systems the constructive interference between such pairs of optical paths is at the origin of modifications to the classical diffusion of waves, such as the coherent backscattering effect [5–11] and the Anderson localization of waves [12,13]. The vectorial nature of electromagnetic waves may actually lead to a reduction of the enhancement of the backscattered signal, as (de)polarization effects kick in [5–7,14,15]. Similarly, the presence of multiple, coupled polarization channels for light has been reported to be detrimental to Anderson localization [16,17], superradiance [18], and subradiance [19], or to the buildup of a large refractive index in dense disordered media [20].

In this Letter, we explore the breaking of reciprocity for light scattered by a disordered medium by introducing noncommuting polarizing optics on the path of the light. The light scattered by a large cold-atom cloud is made to interfere with that from the cloud mirror image, yet the use of a birefringent mirror (M), along with a half-wave plate (P), breaks the symmetry in the transformation that the polarization undergoes on each (reciprocal) path. The reciprocity breaking is monitored through the interference fringes from our mirror-assisted backscattering setup [21], and the reduction of their contrast is shown to derive directly from the lack of commutation of the above-mentioned polarizing optics. While this contrast is associated to the geodesic distance between the polarizations on the Poincaré sphere, the phase difference between them corresponds to the geodesic surface between the injected polarization and the scattered ones (see Fig. 1). This optical phase is known as the Pancharatnam-Berry phase [22,23], and it belongs, as shown by Berry [23], to the broad family of geometric phases that arise in quantum mechanics [24]. In optics, this phase plays an important role to describe wavefront shaping [25–27], especially in the context of light with orbital angular momentum where the manipulation of the optical phase can be interpreted as a form of spin-orbit coupling [28,29]. In our experiment

*Contact author: teixeira@df.ufscar.br

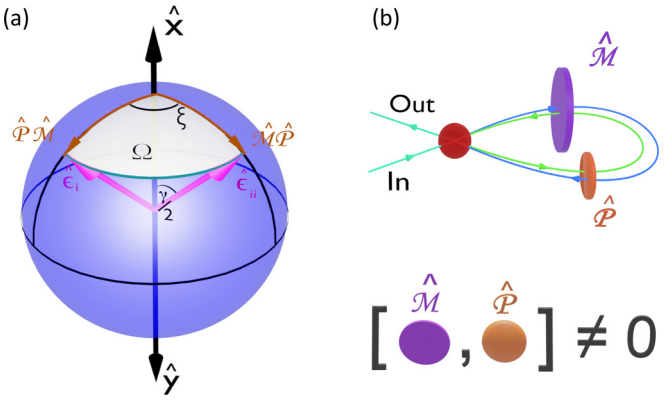

FIG. 1. (a) Representation on the Poincaré sphere of the light polarization $\hat{\epsilon}_i$ and $\hat{\epsilon}_{ii}$, obtained after the successive action of the transformations $\hat{\mathcal{M}}$ and $\hat{\mathcal{P}}$ in direct or reverse order, respectively. The angles ξ and γ are defined by the operations $\hat{\mathcal{M}}$ and $\hat{\mathcal{P}}$, respectively, and the solid angle Ω is indicated in light yellow. (b) Schematic representation of the breaking of reciprocity between time-reversed paths, composed by noncommuting polarization operators $\hat{\mathcal{M}}$ and $\hat{\mathcal{P}}$.

the geometric phase is accessed by measuring the fringe displacement, thus providing a geometrical interpretation to the breaking of reciprocity.

Experimental setup. Our cold-atom setup consists of a cold cloud of $N \approx 3 \times 10^7$ atoms of ^{88}Sr, initially trapped in a magneto-optical trap with a temperature of 10 mK (see Fig. 2). The experiment is performed by turning off the trap, so the atomic cloud expands for a time of flight of 200 μs and reaches a $1/\sqrt{e}$ radius of $R = 1100$ μm. With an associated optical density $b_0 \approx 0.4$, single scattering is dominant. Then,

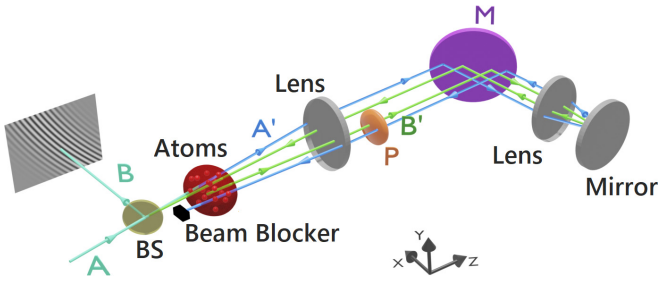

FIG. 2. Experimental setup. The laser light, resonant with the atomic sample, passes through a nonpolarizing beam splitter (BS) before reaching the atomic cloud, which corresponds to path A indicated by a blue arrow. The transmitted beam passes through the 1:1 telescope composed of two lenses of same focal length, is reflected at the 45° mirror M, before being reflected back by a mirror with a small angle θ_0, passing again through a lens, the 45° mirror M, and this time by a half-wave plate P before it reaches the other lens and then atoms; this stands for path A' (in blue). The laser light is finally blocked by a beam blocker, as it accounts for unwanted background in the detected scattered light. The scattered light by the atoms can propagate along the reverse path, where it passes the wave plate before the birefringent mirror and then travels back to the atomic cloud, which corresponds to path B' (in green); from the atomic cloud, the light follows the path B through the BS, to be reflected towards a CCD camera on which one can observe the fringes due to the interference of all the possible paths.

the atoms are probed with a laser beam with a waist $w_0 = 2.1$ mm, so that the intensity is almost homogeneous throughout the cloud. The laser power $P_l = 0.2$ mW, resonant with the 461 nm broad transition of neutral strontium ($\Gamma = 2\pi \times 30.5$ MHz), corresponds to a saturation parameter of $s_0 = 0.07$, so that most of the light is scattered elastically. The pulse duration $t_p = 70$ μs leads to an average number of photons scattered per atom of $N_p = 470$, or to a Doppler displacement of 10 MHz $\approx \Gamma/3$, the actual Doppler displacement being much smaller, since the atoms scatter simultaneously photons from the incoming and retroreflected beam (see Fig. 2 and discussion below).

Our experiment is thus set in the single- and elastic-scattering regime, so the radiation from each atom can be decomposed as four optical paths, composed of the paths A, B, A', and B' shown in Fig. 2. Indeed, the light incoming on the atomic cloud may either:

(i) Follow $A + A' + B$, i.e., cross the atomic sample without being scattered, be reflected on the 45° mirror (M) before being reflected back toward the half-wave plate (P), and finally be scattered by the atoms and reach the CCD.

(ii) Follow $A + B' + B$, i.e., first be scattered by the atoms toward the plate P, then reflected back toward the 45° mirror M, and eventually propagate until the CCD.

(iii) Follow $A + B$, i.e., be directly backscattered by the atoms before being collected on the CCD.

(iv) Follow $A + A' + B' + B$, i.e., cross the science chamber without being deviated, be reflected on the 45° mirror M before being reflected toward the plate P, and be backscattered by the atoms to meet again the plate P, be reflected toward the 45° mirror M, and propagate until the CCD.

In terms of optical paths, the only difference between paths (i) and (ii) is the direction along which the light propagates past the atomic cloud (blue and green paths in Fig. 2), plus a slight variation in optical path as the observation angle is changed. Hence, (i) and (ii) are two reciprocal paths, which interfere to build up fringes (according to the overlap between their polarization). In contrast, (iii) and (iv) correspond to a different optical path for each atom, thus contributing to a background light. Disregarding polarization (that is, when all paths possess the same polarization), this mirror-assisted backscattering configuration [30] can be used to explore the light coherence in disordered atomic clouds [21,31].

Breaking of reciprocity. The polarization of the reciprocal paths is manipulated by using polarizing optics between the cloud and the backscattering mirror (Fig. 2), which breaks the reciprocity of the paths in the following way: The injected light has a linear polarization $\hat{\epsilon}_0 = \hat{x}$. M is a dielectric mirror that induces a phase delay ξ on the $\hat{y}$ component (relative to the $\hat{x}$ component) of the light polarization—this mirror plays the role of a birefringent element, known to induce geometric phases in polarization [32–34]. The fast axis of P is tilted from the $\hat{x}$ axis by an angle $\gamma/2$, which is our control parameter, inducing a reflection of the polarization with respect to the fast axis. Within the Jones formalism for polarizing optics [35,36], the matrices associated to M and P are, respectively,

$$\hat{\mathcal{M}} = \begin{bmatrix} 1 & 0 \\ 0 & e^{i\xi} \end{bmatrix}, \quad \hat{\mathcal{P}} = \begin{bmatrix} \cos\gamma & \sin\gamma \\ \sin\gamma & -\cos\gamma \end{bmatrix}, \tag{1}$$

in the $(\hat{x}, \hat{y})$ basis. Then, the polarizations emerging from each path are given by

$$\hat{\epsilon}_i = \hat{\mathcal{P}}\hat{\mathcal{M}}\hat{\epsilon}_0, \quad \hat{\epsilon}_{ii} = \hat{\mathcal{M}}\hat{\mathcal{P}}\hat{\epsilon}_0,$$
$$\hat{\epsilon}_{iii} = \hat{\epsilon}_0, \quad \hat{\epsilon}_{iv} = \hat{\mathcal{M}}\hat{\mathcal{P}}\hat{\mathcal{P}}\hat{\mathcal{M}}\hat{\epsilon}_0 = \hat{\mathcal{M}}^2\hat{\epsilon}_0. \tag{2}$$

Thus, the polarization of the two paths providing the background light, (iii) and (iv), remain along $\hat{x}$.

The observed fringes result from polarization effects and differences in optical path between the four paths. Indeed, accounting for the tilt between the incident beam after the beam splitter [wave vector $\mathbf{k}_0 = k(\sin\theta_0\hat{y} - \cos\theta_0\hat{z})$] and the backward direction of observation [wave vector $\mathbf{k} = k(\sin\theta\hat{y} + \cos\theta\hat{z})$], we obtain the following field scattered by atom j,

$$\vec{E}_j = E_s\big[e^{ik(\cos\theta-\cos\theta_0)z_j}\hat{\epsilon}_i + e^{ik(\cos\theta_0-\cos\theta)z_j}\hat{\epsilon}_{ii} + e^{ik(\cos\theta_0+\cos\theta)z_j}\hat{\epsilon}_{iii} + e^{-ik(\cos\theta_0+\cos\theta)z_j}\hat{\epsilon}_{iv}\big], \tag{3}$$

where E_s is a prefactor which encapsulates the amplitude of the pump, the single-atom cross section, and the distance of the camera from the setup. Summing the fields from all atoms, and assuming a continuous Gaussian density and a small tilt $|\theta - \theta_0| \ll \theta_0$, we get [37]

$$I_{\text{out}}(\theta) = NI_a\big(1 + \tfrac{1}{2}\text{Re}[\langle\hat{\epsilon}_i, \hat{\epsilon}_{ii}\rangle e^{i\phi}]S_R(\theta)\big), \tag{4}$$

where the scalar product is defined as $\langle\hat{\epsilon}_i, \hat{\epsilon}_{ii}\rangle = \hat{\epsilon}_i \cdot \hat{\epsilon}_{ii}^*$, $\phi = 2\theta_0 kh(\theta - \theta_0)$ the angular variable describing the fringes, with h the distance between the mirror and the center of the atomic cloud, and $S_R(\theta) = e^{-2(\theta_0 kR)^2(\theta-\theta_0)^2}$ the fringes' spatial envelope. Thus, while paths (iii) and (iv) contribute only to the background, the reciprocal paths (i) and (ii) interfere to provide fringes in an angle $|\theta - \theta_0| \lesssim 1/kR$. An example of these fringes and the surrounding background light can be observed in Fig. 2.

Noncommutation of the polarizing optics. As it can be seen in Eq. (4), the fringes with the largest amplitude are observed in the backscattered direction $\theta \approx \theta_0$, and their contrast is given by the modulus of the overlap (that is, the scalar product) between the polarizations of the reciprocal paths (i) and (ii). Let us now discuss how the reduction of this contrast stems directly from the noncommutation of the polarizing elements involved. The role of the (lack of) commutation between the polarizing optics becomes clear when rewriting the scalar product as

$$\langle\hat{\epsilon}_i, \hat{\epsilon}_{ii}\rangle = \langle\hat{\mathcal{P}}\hat{\mathcal{M}}\hat{\epsilon}_0, \hat{\mathcal{M}}\hat{\mathcal{P}}\hat{\epsilon}_0\rangle = 1 - \langle\hat{\mathcal{M}}\hat{\mathcal{P}}\hat{\epsilon}_0, [\hat{\mathcal{P}}, \hat{\mathcal{M}}]\hat{\epsilon}_0\rangle, \tag{5}$$

where $[\cdot, \cdot]$ refers to the commutator. In other words, the interference between the reciprocal paths [see Eq. (4)] is reduced when the matrices of the polarizing optics stop commuting. In the case of M and P used in our experiment, the contrast reads

$$\mathcal{C} = |\langle\hat{\epsilon}_i, \hat{\epsilon}_{ii}\rangle| = \sqrt{1 - \sin^2(2\gamma)\sin^2(\xi/2)}. \tag{6}$$

The delay ξ is determined by the dielectric coating of M, and chosen close to π to maximize the reduction of the contrast [$\xi = (162 \pm 10)^\circ$ in our setup [37]], while γ is used as a control parameter to explore the noncommutation between the optics, and subsequently the breaking of reciprocity between paths (i) and (ii).

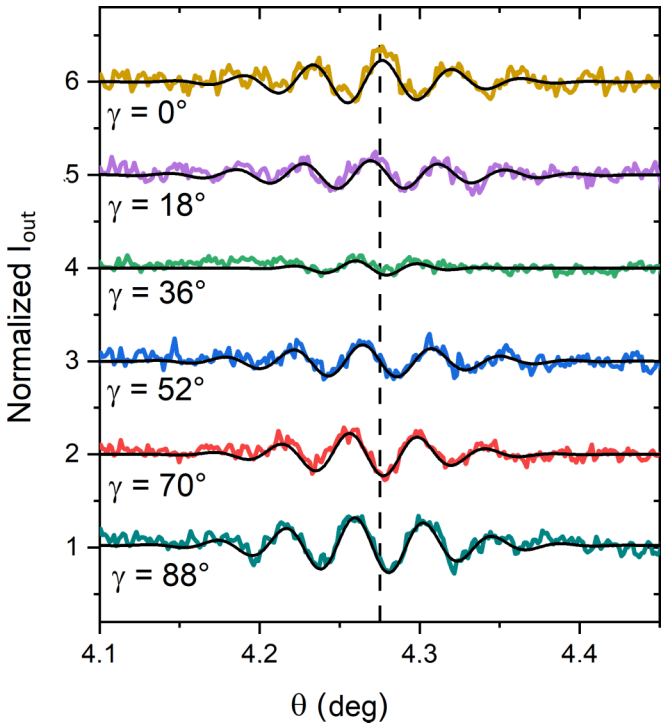

FIG. 3. Colored lines: Interference fringes integrated along the azimuthal direction, normalized to the background intensity, and shifted vertically by one for visibility. Black continuous lines: Fitted fringe profiles, following Eq. (4). Dashed vertical line: Center of the fringes' envelope, θ_0, found by a global fit of the envelope to all curves.

With our experimental apparatus, we measure the scattered light profile at the CCD camera for different angles of the wave plate (i.e., for different values of γ). After over 1000 realizations of the experimental sequence described above, we obtain the light scattered as a function of θ, showing interference fringes that are shown in Fig. 3 (for details on the data analysis and the extraction of the contrast and phase of the fringes, see Supplemental Material [37]). The contrast $\mathcal{C}$ extracted from those fringes is presented in Fig. 4(a), and the minimum observed at $\gamma \approx \pi/4$ is consistent with the prediction from Eq. (6). Note that a better agreement with the experimental data is reached when two effects are accounted for (see the plain red curve). First, the finite optical depth of the cloud is responsible for a larger signal from the background-building path (iii) as compared to the others, which in turn reduces the fringes' contrast. Second, M induces an intensity grating, which depends on the angle γ; then, the finite saturation parameter of the laser affects the fringes' contrast differently depending on this grating [21]. In particular, for $\gamma = \pi/2$ the incident beam and its backreflection possess orthogonal polarization, so the intensity, and thus the saturation parameter, are homogeneous over the cloud. Oppositely, for $\gamma = 0$, the beams have parallel polarizations, which lead to a variation of the saturation parameter over the cloud. The detailed modeling of these effects, and the associated fitting model, are described in Supplemental Material [37].

Pancharatnam-Berry phase and geometrical interpretation. It is clear from the fringes at Fig. 3 that, as the axis of P is

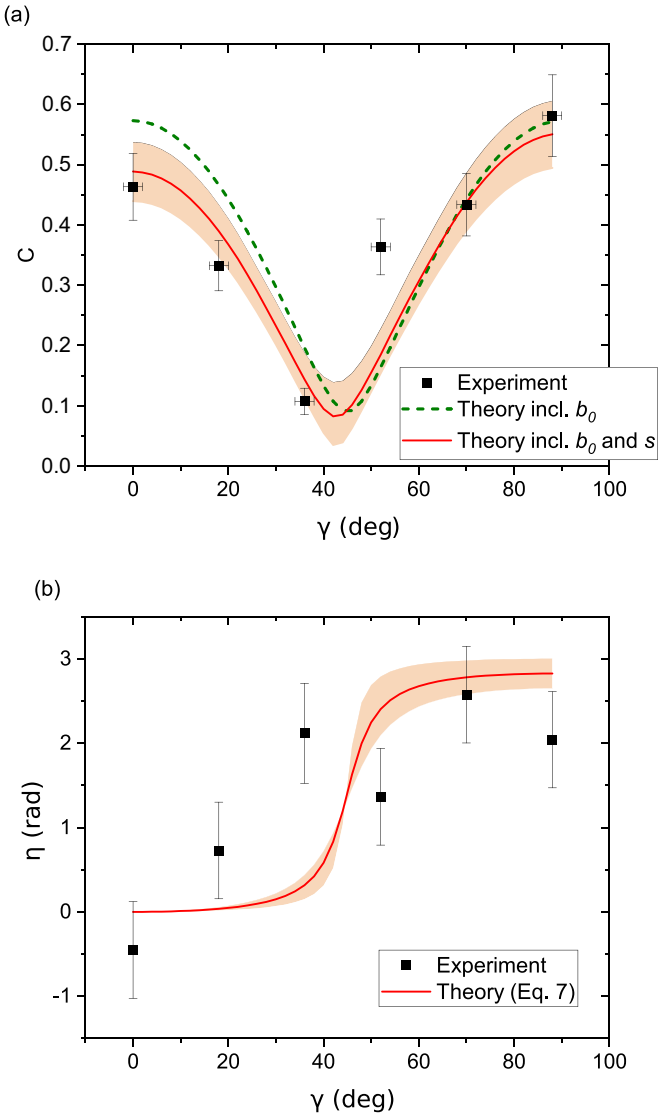

FIG. 4. (a) Contrast derived from the experimental fringes (black squares), from the theoretical prediction (6) once the correction due to the optical thickness of the atomic cloud ($b_0 \approx 0.4$) is included (dashed curve), plus the correction due to the finite saturation parameter of the incoming beam ($s = 0.07$) (continuous curve). The red shaded area corresponds to the confidence interval, which accounts for the uncertainty on the measurement of ξ and on the fitted rescaling factor to account for b_0. (b) Pancharatnam-Berry phase from the experimental fringe displacement (black dots) and from the theoretical prediction (8). The red shaded area corresponds to the confidence interval associated with the uncertainty on the measurement of ξ.

rotated (i.e., as γ is varied), the fringes suffer a reduction in contrast yet they are shifted at the same time. Indeed, if we now consider the phase δ from the scalar product between the polarizations,

$$\langle \hat{\epsilon}_i, \hat{\epsilon}_{ii} \rangle = \mathcal{C} e^{-i\delta}, \tag{7}$$

and incorporate the expression in Eq. (4), then it becomes clear that this phase actually translates into an angular displacement for the fringes. This shift corresponds to the Pancharatnam-Berry phase [22,23], and its geometrical interpretation on the Poincaré sphere is presented in Fig. 1: Starting from the injected polarization $\hat{\epsilon}_0 = \hat{x}$, the light is split into paths (i) and (ii), with its polarization turned into $\hat{\epsilon}_i$ and $\hat{\epsilon}_{ii}$, respectively, before being made to interfere. The solid angle Ω determined by the geodesic triangle $(\hat{\epsilon}_0 \hat{\epsilon}_i \hat{\epsilon}_{ii})$ on the Poincaré sphere corresponds to twice the phase difference between the polarizations $\hat{\epsilon}_i$ and $\hat{\epsilon}_{ii}$ [22], that is, $\delta = -\Omega/2$.

From scalar product (7), we obtain the following equation for the geometrical phase:

$$\tan\delta = \frac{\sin\xi \tan^2\gamma}{1 + \cos\xi \tan^2\gamma}. \tag{8}$$

The measurement of the Pancharatnam-Berry phase presents a fair agreement with the theoretical prediction [see Fig. 4(b)]. The substantial error bars for the experimental data of Fig. 4(b) stem from the uncertainty on the determination of the center of the envelope θ_0. Finally, we note that the contrast also has a geometrical interpretation: It corresponds to $\mathcal{C} = \cos(\zeta/2)$, where ζ is the geodesic distance between the polarizations $\hat{\epsilon}_i$ and $\hat{\epsilon}_{ii}$ on the Poincaré sphere [22].

Conclusions. We have explored the breaking of optical path reciprocity in a mirror-assisted coherent backscattering setup. The fringes emerging from the disordered cold-atom cloud have their contrast reduced as the optical elements used stop commuting and the two interfering paths become nonreciprocal. The measurement of the contrast and angular displacement of the fringes finds their geometrical interpretation on the Poincaré sphere, encapsulated in, respectively, the geodesic distance between the two polarizations and their phase difference, as originally proposed by Pancharatnam and Berry to provide a measure of the difference between polarizations.

In full generality, these results explore the vectorial nature of light to control the reciprocity of two interfering paths, and thus control the interference itself, despite the persisting spectral and spatial coherence. This breaking of reciprocity in the single-scattering regime mimics what happens in multiple scattering regime coherence phenomena, such as the coherent backscattering (CBS) and Anderson localization, when time-reversal symmetry is broken [38–40] via, e.g., the presence of a multilevel Zeeman electronic structure in atoms [11,41,42] or depolarization due to the near-field scattered electric field of close atoms in high densities [16,43]. Interestingly, while the application of a magnetic field can break the time-reversal reciprocity in some cases, it may also restore strong interference phenomena based on the reciprocity of paths, such as for CBS [44] or Anderson localization [45], or as in our setup when the contrast is restored for specific angles of the half-wave plate.

Although our disordered sample is made of saturable atoms subjected to classical (thermal) and quantum (spontaneous emission) decoherence [46], as well as to collective [47,48] or many-body effects [49,50], the role of reciprocity in the light emission is usually hidden within the complexity of the system. Yet the interplay between the polarizations, associated with transitions to different atomic sublevels, could be made explicit, and even controlled, through strategies such as those detailed here or by implementing chiral properties [51–53], with applications, for example, to random lasers [54]. Finally,

for atoms interacting with a Fabry-Pérot cavity where the output results from the interference from several reflection paths, a small nonreciprocal operation, such as a Faraday rotation, on each round trip within the cavity could drastically change the spectrum of the system and alter the lasing properties of extended-cavity diode lasers, with a potential to unveil rich new physics in the different cavity-matter interaction regimes.

Acknowledgments. R.C.T., R.B., and P.W.C. acknowledge funding from Fundação de Amparo à Pesquisa do Estado de São Paulo (FAPESP) through Grants No. 2018/23873-3, No. 2018/15554-5, No. 2022/00261-8, No. 2023/03300-7, No. 2013/04162-5, and No. 2019/13143-0; P.W.C. acknowledges support from the project CAPES-COFECUB Ph879-17/CAPES 88887.130197/2017-01; P.G.S.D., R.K., M.H., R.C.T., R.B., and P.W.C. acknowledge funding from ANR + FAPESP (project QuaCor ANR19-CE47-0014-01/FAPESP 2019/13143-0) and project STIC-AmSud (Ph879-17/CAPES 88887.521971/2020-00) and CAPES-COFECUB (CAPES 88887.711967/2022-00); R.K. and M.H. acknowledge funding from French National Research Agency (ANR) (project PACE-IN ANR19-QUAN-003-01), from European Union's Horizon 2020 research and innovation programme in the framework of Marie Sklodowska-Curie HALT project (Grant Agreement No. 823937), and financial support of the Doeblin Federation; R.K. acknowledges support from the European project ANDLICA, ERC Advanced Grant Agreement No. 832219; M.H. and R.B. acknowledge support by the French government, through the UCAJ.E.D.I. Investments in the Future project managed by the ANR (ANR-15-IDEX-01).

[1] E. Noether, Invariante Variationsprobleme, Nachr. Ges. Wiss. Gottingen, Math.-Phys. Kl. **1918**, 235 (1918).
[2] E. Noether, Invariant variation problems, Transport Theory Stat. Phys. **1**, 186 (1971).
[3] R. J. Potton, Reciprocity in optics, Rep. Prog. Phys. **67**, 717 (2004).
[4] R. Carminati, J. J. Sáenz, J.-J. Greffet, and M. Nieto-Vesperinas, Reciprocity, unitarity, and time-reversal symmetry of the *S* matrix of fields containing evanescent components, Phys. Rev. A **62**, 012712 (2000).
[5] Y. Kuga and A. Ishimaru, Retroreflectance from a dense distribution of spherical particles, J. Opt. Soc. Am. A **1**, 831 (1984).
[6] P.-E. Wolf and G. Maret, Weak localization and coherent backscattering of photons in disordered media, Phys. Rev. Lett. **55**, 2696 (1985).
[7] M. P. Van Albada and A. Lagendijk, Observation of weak localization of light in a random medium, Phys. Rev. Lett. **55**, 2692 (1985).
[8] K. M. Yoo, G. C. Tang, and R. R. Alfano, Coherent backscattering of light from biological tissues, Appl. Opt. **29**, 3237 (1990).
[9] M. I. Mishchenko, On the nature of the polarization opposition effect exhibited by Saturn's rings, Astrophys. J. **411**, 351 (1993).
[10] A. Tourin, A. Derode, P. Roux, B. A. van Tiggelen, and M. Fink, Time-dependent coherent backscattering of acoustic waves, Phys. Rev. Lett. **79**, 3637 (1997).
[11] G. Labeyrie, F. de Tomasi, J.-C. Bernard, C. A. Müller, C. Miniatura, and R. Kaiser, Coherent backscattering of light by cold atoms, Phys. Rev. Lett. **83**, 5266 (1999).
[12] P. W. Anderson, Absence of diffusion in certain random lattices, Phys. Rev. **109**, 1492 (1958).
[13] E. Akkermans and G. Montambaux, *Mesoscopic Physics of Electrons and Photons* (Cambridge University Press, Cambridge, UK, 2007).
[14] E. Akkermans, P. E. Wolf, and R. Maynard, Coherent backscattering of light by disordered media: Analysis of the peak line shape, Phys. Rev. Lett. **56**, 1471 (1986).
[15] M. J. Stephen and G. Cwilich, Rayleigh scattering and weak localization: Effects of polarization, Phys. Rev. B **34**, 7564 (1986).
[16] S. E. Skipetrov and I. M. Sokolov, Absence of Anderson localization of light in a random ensemble of point scatterers, Phys. Rev. Lett. **112**, 023905 (2014).
[17] C. E. Máximo, N. Piovella, P. W. Courteille, R. Kaiser, and R. Bachelard, Spatial and temporal localization of light in two dimensions, Phys. Rev. A **92**, 062702 (2015).
[18] M. Gross and S. Haroche, Superradiance: An essay on the theory of collective spontaneous emission, Phys. Rep. **93**, 301 (1982).
[19] A. Cipris, R. Bachelard, R. Kaiser, and W. Guerin, van der Waals dephasing for Dicke subradiance in cold atomic clouds, Phys. Rev. A **103**, 033714 (2021).
[20] F. Andreoli, M. J. Gullans, A. A. High, A. Browaeys, and D. E. Chang, Maximum refractive index of an atomic medium, Phys. Rev. X **11**, 011026 (2021).
[21] P. H. Moriya, R. F. Shiozaki, R. Celistrino Teixeira, C. E. Máximo, N. Piovella, R. Bachelard, R. Kaiser, and P. W. Courteille, Coherent backscattering of inelastic photons from atoms and their mirror images, Phys. Rev. A **94**, 053806 (2016).
[22] S. Pancharatnam, Generalized theory of interference, and its applications, Proc. Indian Acad. Sci. Sect. A **44**, 247 (1956).
[23] M. Berry, The adiabatic phase and Pancharatnam's phase for polarized light, J. Mod. Opt. **34**, 1401 (1987).
[24] E. Cohen, H. Larocque, F. Bouchard, F. Nejadsattari, Y. Gefen, and E. Karimi, Geometric phase from Aharonov–Bohm to Pancharatnam–Berry and beyond, Nat. Rev. Phys. **1**, 437 (2019).
[25] Z. Bomzon, G. Biener, V. Kleiner, and E. Hasman, Space-variant Pancharatnam–Berry phase optical elements with computer-generated subwavelength gratings, Opt. Lett. **27**, 1141 (2002).
[26] G. Biener, A. Niv, V. Kleiner, and E. Hasman, Formation of helical beams by use of Pancharatnam–Berry phase optical elements, Opt. Lett. **27**, 1875 (2002).
[27] D. Lin, P. Fan, E. Hasman, and M. L. Brongersma, Dielectric gradient metasurface optical elements, Science **345**, 298 (2014).
[28] L. Marrucci, C. Manzo, and D. Paparo, Optical spin-to-orbital angular momentum conversion in inhomogeneous anisotropic media, Phys. Rev. Lett. **96**, 163905 (2006).
[29] E. Brasselet, N. Murazawa, H. Misawa, and S. Juodkazis, Optical vortices from liquid crystal droplets, Phys. Rev. Lett. **103**, 103903 (2009).

[30] J. J. Greffet, Backscattering of *S*-polarized light from a cloud of small particles above a dielectric substrate, Waves Random Media **1**, S65 (1991).

[31] P. G. S. Dias, M. Frometa, P. H. N. Magnani, K. R. B. Theophilo, M. Hugbart, P. W. Courteille, and R. C. Teixeira, Mirror-assisted backscattering interferometry to measure the first-order correlation function of the light emitted by quantum scatterers, Phys. Rev. A **104**, 053716 (2021).

[32] M. V. Berry and S. Klein, Geometric phases from stacks of crystal plates, J. Mod. Opt. **43**, 165 (1996).

[33] R. Bhandari, Polarization of light and topological phases, Phys. Rep. **281**, 1 (1997).

[34] R. Simon, H. J. Kimble, and E. C. G. Sudarshan, Evolving geometric phase and its dynamical manifestation as a frequency shift: An optical experiment, Phys. Rev. Lett. **61**, 19 (1988).

[35] R. C. Jones, A new calculus for the treatment of optical systems. I. Description and discussion of the calculus, J. Opt. Soc. Am. **31**, 488 (1941).

[36] E. Collett, Equation summary, in *Field Guide to Polarization* (SPIE, Bellingham, WA, 2009), pp. 114–123.

[37] See Supplemental Material at http://link.aps.org/supplemental/10.1103/PhysRevA.110.L041302 for details on the derivation of the equations of the article, on details of the experimental protocol, and on data treatment.

[38] T. Micklitz, C. A. Müller, and A. Altland, Echo spectroscopy of Anderson localization, Phys. Rev. B **91**, 064203 (2015).

[39] K. Müller, J. Richard, V. V. Volchkov, V. Denechaud, P. Bouyer, A. Aspect, and V. Josse, Suppression and revival of weak localization through control of time-reversal symmetry, Phys. Rev. Lett. **114**, 205301 (2015).

[40] C. Hainaut, I. Manai, J.-F. Clément, J. C. Garreau, P. Szriftgiser, G. Lemarié, N. Cherroret, D. Delande, and R. Chicireanu, Controlling symmetry and localization with an artificial gauge field in a disordered quantum system, Nat. Commun. **9**, 1382 (2018).

[41] C. A. Müller, T. Jonckheere, C. Miniatura, and D. Delande, Weak localization of light by cold atoms: The impact of quantum internal structure, Phys. Rev. A **64**, 053804 (2001).

[42] G. Labeyrie, C. Miniatura, C. A. Müller, O. Sigwarth, D. Delande, and R. Kaiser, Hanle effect in coherent backscattering, Phys. Rev. Lett. **89**, 163901 (2002).

[43] L. Bellando, A. Gero, E. Akkermans, and R. Kaiser, Cooperative effects and disorder: A scaling analysis of the spectrum of the effective atomic Hamiltonian, Phys. Rev. A **90**, 063822 (2014).

[44] O. Sigwarth, G. Labeyrie, T. Jonckheere, D. Delande, R. Kaiser, and C. Miniatura, Magnetic field enhanced coherence length in cold atomic gases, Phys. Rev. Lett. **93**, 143906 (2004).

[45] S. E. Skipetrov and I. M. Sokolov, Magnetic-field-driven localization of light in a cold-atom gas, Phys. Rev. Lett. **114**, 053902 (2015).

[46] P. Lassègues, M. A. F. Biscassi, M. Morisse, A. Cidrim, P. G. S. Dias, H. Eneriz, R. C. Teixeira, R. Kaiser, R. Bachelard, and M. Hugbart, Transition from classical to quantum loss of light coherence, Phys. Rev. A **108**, 042214 (2023).

[47] S. J. Roof, K. J. Kemp, M. D. Havey, and I. M. Sokolov, Observation of single-photon superradiance and the cooperative Lamb shift in an extended sample of cold atoms, Phys. Rev. Lett. **117**, 073003 (2016).

[48] W. Guerin, M. O. Araújo, and R. Kaiser, Subradiance in a large cloud of cold atoms, Phys. Rev. Lett. **116**, 083601 (2016).

[49] E. Urban, T. A. Johnson, T. Henage, L. Isenhower, D. Yavuz, T. Walker, and M. Saffman, Observation of Rydberg blockade between two atoms, Nat. Phys. **5**, 110 (2009).

[50] A. Cidrim, T. S. do Espirito Santo, J. Schachenmayer, R. Kaiser, and R. Bachelard, Photon blockade with ground-state neutral atoms, Phys. Rev. Lett. **125**, 073601 (2020).

[51] R. Mitsch, C. Sayrin, B. Albrecht, P. Schneeweiss, and A. Rauschenbeutel, Quantum state-controlled directional spontaneous emission of photons into a nanophotonic waveguide, Nat. Commun. **5**, 5713 (2014).

[52] P. Lodahl, S. Mahmoodian, S. Stobbe, A. Rauschenbeutel, P. Schneeweiss, J. Volz, H. Pichler, and P. Zoller, Chiral quantum optics, Nature (London) **541**, 473 (2017).

[53] Y.-T. Chen, L. Du, L. Guo, Z. Wang, Y. Zhang, Y. Li, and J.-H. Wu, Nonreciprocal and chiral single-photon scattering for giant atoms, Commun. Phys. **5**, 215 (2022).

[54] D. S. Wiersma, The physics and applications of random lasers, Nat. Phys. **4**, 359 (2008).